Brassinosteroid and CLASP-driven Models of Root Zonation in *A. Thaliana*

Riley Wheadon, Geoffrey Wasteneys, Eric Cytrynbaum
University of British Columbia

September 8th, 2024

1 Abstract

The distinct zones of cell beahviour observed in the roots of *A. thaliana* play an essential role in maintaining optimal levels of growth. In this paper, we use recent research on brassinosteroids and the CLASP1 protein to develop two novel mathematical models of the zonation phenomenon. Our first model explains differences in behaviour in the epidermal cells of the wild type root of *A thaliana* when compared two mutant roots in which elements of the CLASP1 signalling network have been perturbed. We find that length-based mechanism for cell division is sufficient to qualitatively explain the zonation patterns of these mutants. Then we present a model of a single cell in the wild type root fitted to levels of BR singalling levels and cell length from experimental observations. We discuss the benefits and drawbacks of this model and identify avenues for further study.

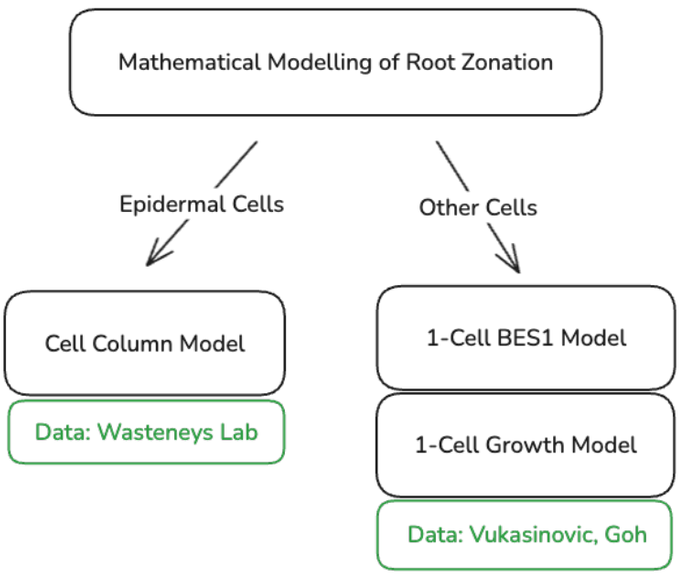

Figure 1: An overview of the models presented in this paper.

2 Introduction

2.1 Root Zonation

The growing root of *A. thaliana* can be roughly divided into six distinct zones, with the cells in each zone exhibiting qualitatively distinct behaviour. At the tip of the root lies the root cap, a region of cells that are constantly sluffed off to protect the growing root from debris (Kumpf and Nowack, 2015). Above the root cap is a small group of static cells known as the quiescent centre (henceforth QC), which play a crucial role in the regeneration of the root cap and surrounding cells (Matosevich and Efroni, 2021). The models presented in this paper will ignore these two regions and measure position within the root as the distance in µm from the QC.

In the meristematic zone (henceforth MZ), cells experience rapid cell division and slower cell growth. In this region, cells grow from 4.5µm to 9µm over a period of about 18h (Verbelen et al., 2006) while moving from 0µm to 200µm above the QC. Above the meristematic zone is the transition zone (henceforth TZ), in which cells grow from 9µm to 30µm over the course of 10h (Verbelen et al., 2006). Microscopy imaging found the CDC2 protein kinase in epidermal cells in the distal region of the TZ, which suggests that some cells in the TZ have the capacity for division (Verbelen et al., 2006). The TZ spans from approximately 200µm to 520µm above the QC. Next to the TZ is the elongation zone (henceforth EZ), where cells grow rapidly from 30µm to 130µm over the course of 4h (Verbelen et al., 2006). After leaving the EZ at approximately 900µm above the QC, cells begin differentiation and cease growth. Thus the final and most proximal region of the root is aptly named the differentiation zone (henceforth DZ).

2.2 CLASP and Microtubules

Microtubules (henceforth MTs) are tubulin polymers located on the plasma membrane of the cell which guide the deposition of cellulose on the cell wall (Hamant and Traas, 2010). When the MTs and cellulose microfibrils are deposited orthogonally to the axis of growth, the cell experiences anisotropic growth. If the MTs and cellulose are less organized, then the turgor pressure within the cell faces isotropic resistance which ultimately inhibits growth (Hamant and Traas, 2010).

The CLASP protein plays an essential role in MT patterning through its ability to help MTs cross sharp edges on the cell membrane (C. Ambrose et al., 2011). This results formation of bundles of MTs along the transverse, radial, and longitudinal edges of the cell (Halat et al., 2022). Bundles along the transverse and radial edges (henceforth TFBs), are of particular interest because they lead to microtubule arrangements that run parallel to the axis of growth. These TFBs disrupt the formation of circumferential cellulose microfibrils, which ultimately inhibits cell growth (Halat et al., 2022). Cell length modulates the effect of CLASP on MT patterning due to the fact that longer cells have longer longitudinal edges relative to their radial and transverse edges. Therefore, the CLASP protein to localizes towards the longitudinal edges and away from the radial and transverse edges in longer cells, leading to a reduction in TFBs and an increase in growth (Halat et al., 2022).

2.3 Brassinosteroid

Brassinosteroids (BRs) are a class of plant hormones that have shown to promote both longitudinal and radial growth in a spatiotemporal manner (Ackerman-Lavert and Savaldi-Goldstein, 2020). Extracellular BRs, particularly brassinoslide (henceforth BL), bind to the BR receptor BRI1 and its homologues on the cell membrane (Vukašinović et al., 2021). This releases the inhibition of the BZR1/BES1 transcription factors by the BIN2 signalling inhibitor (Ackerman-Lavert and Savaldi-Goldstein, 2020). The effects of BR signalling have been shown to be stronger in the TZ and stronger still in the EZ due to a higher concentration of BR precursors (Vukašinović et al., 2021).

The BZR1/BES1 transcription factors, which are often used as a proxy for BR signalling, have been shown to inhibit CLASP by binding directly to its promoter and repressing its activity (Ruan et al., 2018). Additionally, CLASP influences the BR signalling network by promoting the recycling of endocytosed BRI1 receptors. Together, these two effects produce a stable postive-negative feedback loop that helps to ensure homeostasis in the root (Ruan et al., 2018).

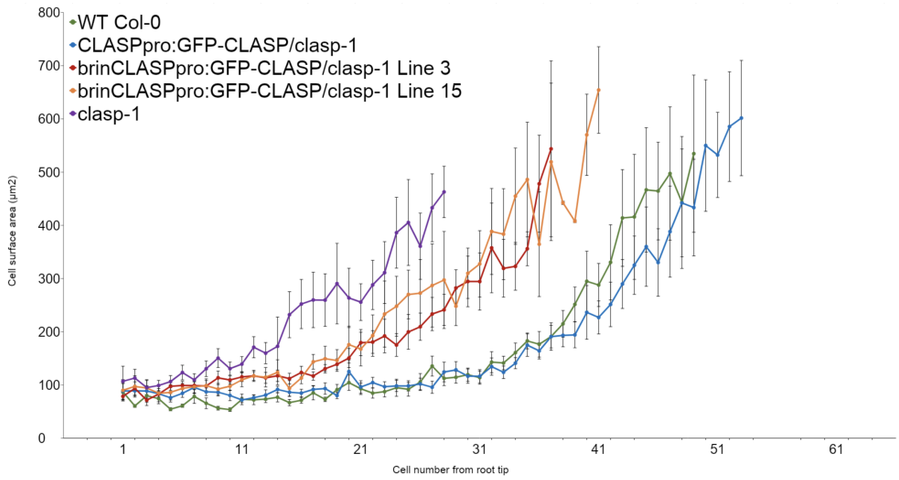

Figure 2: Average cell areas plotted against cell number for each of the two mutant roots and the wild type. The GFP-CLASP line drives the expression of a fluorescent fusion protein which fully complements the CLASP-1 mutant (C. Ambrose et al., 2011). Therefore, the GFP-CLASP/clasp-1 root is phenotypically similar to the wild type. Observe that the CLASP-1 mutant has the largest cells, followed by the BRIN-CLASP mutant, followed by the wild type.

2.4 Mutant Roots

Making small changes to the network of proteins and hormones described in the prior two sections leads to significant changes in root phenotypes. This paper explores the *clasp-1* (henceforth CLASP-1) (J. C. Ambrose et al., 2007) and *brinCLASPpro* (henceforth BRIN-CLASP) (Ruan et al., 2018) mutant roots. The CLASP-1 root has a loss-of-function mutation that entirely inhibits the production of CLASP, which ultimately leads to an increase in cell growth through the previously discussed pathway (Halat et al., 2022). However, the rapid cell growth results in fewer cell divisions and thus fewer cells in the CLASP-1 root (Halat et al., 2022), resulting in a lower rate of overall root growth relative to the wild type (J. C. Ambrose et al., 2007).

In wild type roots, the transcription of the CLASP protein is inhibited whenthe root is exposed to exogenous BRs (Ruan et al., 2018). However, the BRIN-CLASP root is insensitive to the effects of BR signalling, meaning the application of exogenous BRs does not affect the amount of CLASP in this mutant. It therefore stands to reason that the BRIN-CLASP mutant should have more CLASP than the wild type due to the abscence of this inhibition. It has been shown that an excess of CLASP upregulates the level of BR signalling by promoting the recycling of BRI1 receptors (Ruan et al., 2018), and we speculate that this leads to the increased cell growth observed in BRIN-CLASP mutants relative to the wild type. A plot of cell size in trichoblast cells from the mutants and the wild type is shown in Figure 2.

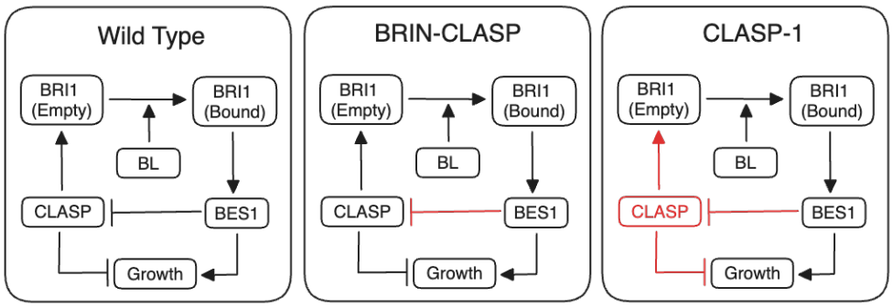

Figure 3: Signalling network in the wild type, BRIN-CLASP mutant, and CLASP-1 mutant. Red arrows denote signalling pathways that were removed due to the mutation.

3 Cell Column Model

Our first model of CLASP-driven root growth in *A. thaliana* aims to qualitatively explain the phenomenon of cell zonation. A quantitative analysis of the differences in behaviour between the mutants is presented in Supplementary Figure 1 and 2. In this model, each cell has a length L which increases with time. Every cell also has a division level D. When $D > 1$, the cell divides into two cells with length $L/2$ and division level $D = 0$. We model the changes in L and D over an arbitrary time scale using a number of assumptions described in the subsequent paragraphs.

A cell can divide every $1/d_0$ time units at most. Cells must be at least 9µm long in order to divide (Verbelen et al., 2006). The cell division rate is inhibited by the length of the cell. By making this assumption, we treat cell length as a proxy for the levels of the various hormones that truly drive cell division. We also make the assumption that the CLASP-1 and BRIN-CLASP mutations do not modulate progress in the cell cycle directly. In other words, the dD/dt equation is identical for the wild type, CLASP-1, and BRIN-CLASP models. This assumption may very well be incorrect, but it is sufficient to explain the observed data.

Next, we let cells grow at a basal rate g_0. The BRIN-CLASP mutant and wild-type root have their basal growth rate decreased due to the presence of CLASP-driven microtubule bundles that run parallel to the axis of growth. Additionally, cells further from the QC grow at a faster rate due to the increased concentration of extracellular BL, which leads to higher levels of BES1 signalling. The CLASP-1 mutant and wild-type root have their position-dependent growth rate reduced by the fact that lower CLASP levels (compared to the BRIN-CLASP mutant) reduces the number of BRI1 receptors on the cell membrane which in turn leads to lower BES1 signalling levels. Cells also have a maximum size of $150\mu m$ which comes from the "Sizer" model for cell differentiation presented by Pavelescu et al., 2018 combined with observations from Verbelen et al., 2006 and our experimental data.

To determine the exact equations used in the cell column model we need to take a closer look at the singalling network in the various mutants shown in Figure 3. Observing the pathways in each mutant indicates that the CLASP level should be highest in the BRIN-CLASP mutant (since CLASP is not repressed by BES1), followed by the wild type, followed by the CLASP-1 mutant (which has no CLASP at all). Since CLASP promotes the recycling of BRI1 receptors, the number of receptors should also be highest in the BRIN-CLASP mutant, followed by the wild type, followed by the CLASP-1 mutant. Let C_{WT} and C_{BC} denote the level of CLASP in the wild type and BRIN-CLASP roots respectively. Similarly, define R_{WT}, R_{BC}, and R_{C1} for the receptor levels. Using these variables we can define the equations for the model shown in Equation (1).

$$\begin{aligned}
\frac{dL_{\mathrm{C1}}}{dt} &= ((g_0 - 0) + R_{\mathrm{C1}}P)L, & \frac{dD}{dt} &= d_0\left(1 - \frac{L^n}{d_L^n + L^n}\right) \\
\frac{dL_{\mathrm{BC}}}{dt} &= ((g_0 - C_{\mathrm{BC}}) + R_{\mathrm{BC}}P)L, & \frac{dD}{dt} &= d_0\left(1 - \frac{L^n}{d_L^n + L^n}\right) \\
\frac{dL_{\mathrm{WT}}}{dt} &= ((g_0 - C_{\mathrm{WT}}) + R_{\mathrm{WT}}P)L, & \frac{dD}{dt} &= d_0\left(1 - \frac{L^n}{d_L^n + L^n}\right)
\end{aligned} \tag{1}$$

Parameter	Units	Value
g_0	$1/t$	0.02500
c_{WT}	$1/t$	0.01400
c_{BC}	$1/t$	0.02200
R_{C1}	$1/(\mu\mathrm{m} \cdot t)$	0.00028
R_{WT}	$1/(\mu\mathrm{m} \cdot t)$	0.00029
R_{BC}	$1/(\mu\mathrm{m} \cdot t)$	0.00030
d_0	D/t	0.05000
d_L	µm	20.0000
n	1	20.0000

Table 1: Parameter values for cell column model.

Model	Mean Div.	Median Div.	Max Div.	# Divs.
Wild Type	158.51	151.41	344.34	537
BRIN-CLASP	138.26	131.49	307.45	523
CLASP-1	96.28	83.80	241.98	396

Table 2: Division behaviour in cell column models.

As discussed previously, these equations are subject to the restrictions $0 < C_{\mathrm{WT}} < C_{\mathrm{BC}}$ and $R_{\mathrm{C1}} < R_{\mathrm{WT}} < R_{\mathrm{BC}}$. We ran the model with a time step 0.01 for a period of $T = 500$ arbitrary units. The simulations were initialized with 10 cells of length 7µm. Parameters were fitted by hand to match an exponential curve fitted to experimentally observed data. The results of these simulations are shown in Figure 4. For more information, see the supplementary figures in the appendix. The parameters used in all of the figures presented are shown in Table 1 while information about division behaviour is shown in Table 2.

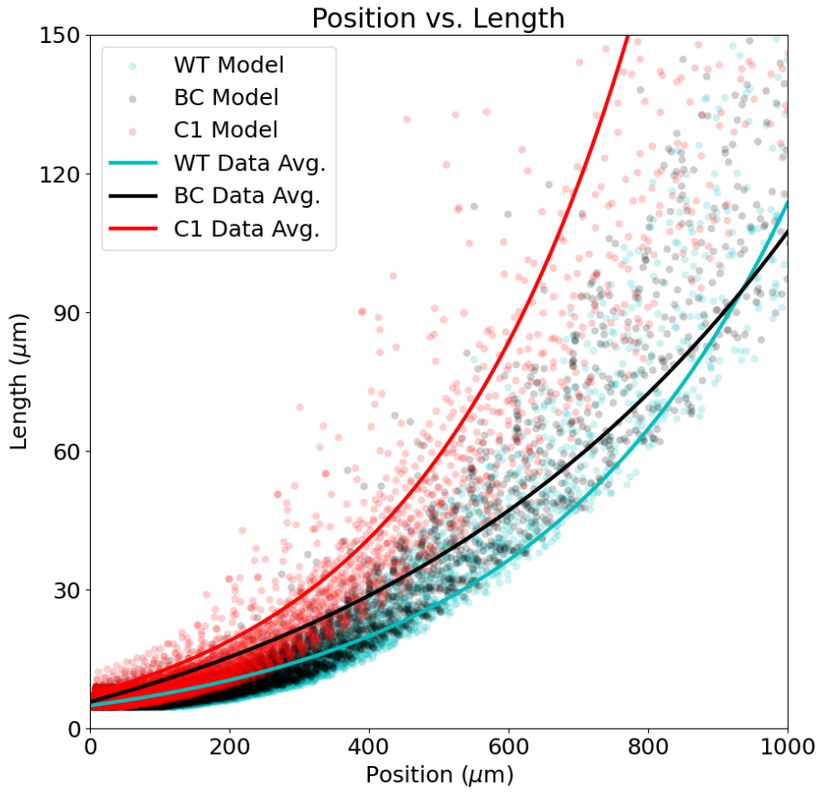

Figure 4: Position vs. length data from the model compared with experimental observations.

4 Single Cell BES1 Model

4.1 Brassinoslide Component

Vukašinović et al., 2021 provide a detailed biosynthetic pathway for BL by outlining how campestrol undergoes multiple chemical reactions to eventually form BL. The biosynthetic enzymes DWF4, CPD, DET3, ROT3, BR6OX1, and BR6OX2 catalyze these reactions. Mutants made to be deficient in each of the aforementioned enzymes exhibited stunted growth, which shows that these enzymes are crucial for effective BL synthesis. The biosynthetic enzymes CPD and ROT3 were observed by Vukašinović et al., 2021 using fluorescence imaging in the vascular cell columns of a single root. They found that both CPD and ROT3 remain relatively constant in the meristem (0-200µm) before increasing in the transition zone (200-400µm) and reaching a maximum in the early elongation zone (400-700µm). After 700µm, the CPD and ROT3 levels began to decrease.

Since BL is the most biosynthetically active brassinosteroid, we make the assumption that it is the only brassinosteroid present in the root. Additionally, we assume that the fluorescence intensity of CPD and ROT3 measured by (Vukašinović et al., 2021) are equivalent to the concentration of BL ligand up to some scalar multiple. To determine this scalar, we use an estimate from van Esse et al., 2012 that gives the extracellular concentration of BL ligand to be at most $1\text{nmol}\,\text{L}^{-1}$in wild-type roots. This gives us the following formula for the extracellular BL concentration [BL] in $\text{nmol}\,\text{L}^{-1}$:

$$[\text{BL}] = b \cdot \frac{\text{CPD}}{\max(\text{CPD})} + (1-b) \cdot \frac{\text{ROT3}}{\max(\text{ROT3})} \tag{2}$$

In (2), the parameter $b \in [0,1]$ controls the bias towards CPD in order to account for the fact that the exact details of the BL pathway are omitted from our model. Using the data from Vukašinović et al., 2021 along with (2), we plotted the BL concentration against position for different levels of bias (see Supplementary Figure 8). Since the functions behaved qualitatively the same, we assigned $b = 0.5$. Additionally, BR biosynthetic enzymes have been shown to move short distances in

the root (Vukašinović et al., 2021), so we take an $n\,\mu$m moving average of the BL concentration function to account for diffusion. Shown in Supplementary Figure 9 is a plot of the BL concentration function for different values of n. We settled on $n = 50\mu$m as a reaosnable estimate of this diffusive effect.

4.2 BRI1 Receptor Component

From the description of the BL concentration function in Equation (2) we can derive a formula for the concentration of bound BRI1 receptors at any position in the root. To do this, we use the equilibrium and mass-balance equations for the BRI1 receptor network introduced by van Esse et al., 2012.

$$[\text{BRI1 BL}] = \frac{[\text{BRI1}_{\text{free}}] \cdot [\text{BL}_{\text{free}}]}{K_d} \tag{3}$$

$$\begin{aligned} [\text{BRI1}] &= [\text{BRI1 BL}] + [\text{BRI1}_{\text{free}}] \\ [\text{BL}] &= [\text{BRI1 BL}] + [\text{BL}_{\text{free}}] \end{aligned} \tag{4}$$

In the equations above, [BRI1 BL] denotes the concentration of bound BRI1 receptors, which are assumed to bind at a ratio of one molecule to one monomer (van Esse et al., 2012). K_d is the BL dissociation constant. Additionally, $[\text{BRI1}_{\text{free}}]$ and $[\text{BL}_{\text{free}}]$ denote the unbound BRI1 and BL concentrations respectively, while [BL] and [BRI1] represent the total BRI1 and BL concentrations. To further simplify our model, we can express [BRI1 BL] as a function of [BRI1] and [BL] by substituting (4) into (3) to get:

$$[\text{BRI1 BL}] = \frac{([\text{BRI1}] - [\text{BRI1 BL}])([\text{BL}] - [\text{BRI1 BL}])}{K_d} \tag{5}$$

$$K_d \cdot [\text{BRI1 BL}] = [\text{BRI1}] \cdot [\text{BL}] - ([\text{BL}] + [\text{BRI1}]) \cdot [\text{BRI1 BL}] + [\text{BRI1 BL}]^2 \tag{6}$$

$$[\text{BRI1 BL}]^2 - ([\text{BL}] + [\text{BRI1}] + K_d) \cdot [\text{BRI1 BL}] + ([\text{BRI1}] \cdot [\text{BL}]) = 0 \tag{7}$$

Now, we can use the quadratic formula to determine the positive value of [BRI1 BL] for which (7) holds. This gives us a formula for [BRI1 BL] in terms of [BRI1] and [BR], where $A = ([\text{BL}] + [\text{BRI1}] + K_d)$.

$$[\text{BRI1 BL}] = \frac{A - \sqrt{A^2 - 4 \cdot [\text{BRI1}] \cdot [\text{BL}]}}{2} \tag{8}$$

Empirical research gives us estimates for the values of [BRI1] and K_d. van Esse et al., 2012 estimate the BRI1 receptor concentration to be $62 \pm 4\text{nmol}\,\text{L}^{-1}$ in wild type roots. Values for the BL dissociation constant K_d range from $7.4\text{nmol}\,\text{L}^{-1}$ to $15\text{nmol}\,\text{L}^{-1}$ (Wang et al., 2001) up to $55\text{nmol}\,\text{L}^{-1}$ (Caño-Delgado et al., 2004). For the models presented in the forthcoming sections, we will take $[\text{BRI1}] = 62\text{nmol}\,\text{L}^{-1}$ and $K_d = 10\text{nmol}\,\text{L}^{-1}$. Using these parameters along with the formula in equation (8) we get the [BRI1 BL] function shown in Figure 5.

Our model makes the assumption that all BRI1 receptors are localized to the cell membrane. Additionally, it assumes that the law of mass action is a reasonable approximation for the diffusing BL ligand binding to the static BRI1 receptors. We believe this decision is justified due to the low percentage occupancy of the BRI1 receptors, which suggests that any free BL ligand will have many oppourtunities to bind to a receptor. Further modelling of the BRI1 receptor network using the physical properties of the system would help to clarify and refine these assumptions.

4.3 BES1 Signalling Model

In this model and all subsequent models we aim to predict the behaviour of a single cell as it is pushed away from the quiescent centre (henceforth QC) by the growth and division of the cells beneath it. Within the meristematic zone, cells grow from a length of 4.5µm to 9µm over a period of approximately 18h (Verbelen et al., 2006). However, cells may undergo one or more divisions during this time (Goh et al., 2023), so tracking the exact lineage of a single cell is difficult. For this reason, our model will only consider cells at 150µm or higher above the QC.

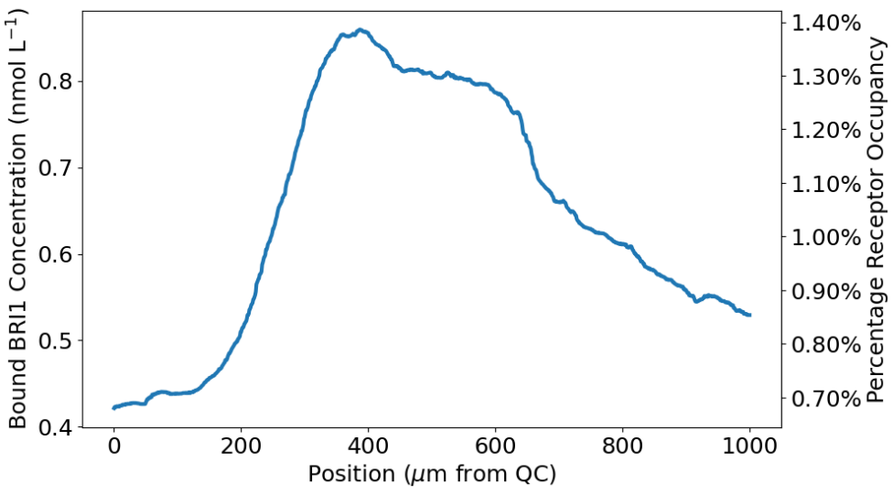

Figure 5: Plot of bound receptor concentration (left axis) measured in nmol L^{-1} as well as receptor occupancy percentage (right axis). Due to the fact that [BL] $\ll$ [BRI1] the [BRI1 BL] function is approximately equal to the [BL] function up to some scalar multiple.

Prior to writing down a system of differential equations for our model, we need to rescale our data to be in terms of time instead of position. To do this, we map a position of 150µm above the QC to $t = 0$h and then use cell lineage data from Goh et al., 2023 to determine a function that maps positions to times. The resulting position function is shown in Supplementary Figure 10.

Our first model aims to predict the level of BR signalling within the cell as it moves away from the QC, measured in terms of the BES1 transcription factor. To do this, we will use a time-rescaled version of the BL concentration function shown in Supplementary Figures 8 and 9 with $b = 0.5$ and $n = 50$. The model will be fit to time-rescaled fluorescence intensity data from the cell columns of a single *A. thaliana* root (Vukašinović et al., 2021). The BL concentration function and the data are shown in Supplementary Figure 11. It is important to note that there is likely additional plant-to-plant variance that remains unaccounted for due to the fact that the data comes from a single organism.

With our data prepared, we can now define an ODE model for the amount of BES1 transcript in terms of the BL concentration $B(t) = [\mathrm{BL}]$. To do this, recall that Equation (8) gives us the concentration of bound BRI1 receptors $R_B = [\mathrm{BRI1\ BL}]$ in terms of $B(t)$, the dissociation constant K_d, and the total BRI1 concentration $R_T = [\mathrm{BRI1}]$. For this model, we will fix $K_d = 10\mathrm{nmol\,L}^{-1}$ (Wang et al., 2001) and $R_T = 62\mathrm{nmol\,L}^{-1}$ (van Esse et al., 2012) as in Figure 5.

$$R_B(B, R_T, K_d) = \frac{(B + R_T + K_d) - \sqrt{(B + R_T + K_d)^2 - 4 \cdot R_T \cdot B}}{2} \tag{9}$$

When the concentration of bound BRI1 receptors R_B is higher, the effects of the BIN2 signalling inhibitor are released, leading to increased production of BES1. Let s_{in} denote the rate at which R_B increases BES1 transcription. We also include a decay term with parameter s_{out} to account for the degradation of the BES1 transcription factor over time. The intial condition is given by another parameter $\mathrm{BES1}(0) = s_0$. Fitting this parameter will give us a non-dimensional estimate for the level of BES1 signalling at 150µm above the QC.

$$\frac{d\mathrm{BES1}}{dt} = s_{\mathrm{in}} R_B(B, R_T, K_d) - s_{\mathrm{out}}\mathrm{BES1}, \quad \mathrm{BES1}(0) = s_0 \tag{10}$$

Since R_B has t-dependence through the BL concentration function B, Equation (10) cannot be solved analytically and must be approximated using numerical methods. Before we show the results of these simulations, we present a visual summary of the model in Figure 6.

The BES1 function was approximated using a forward euler method with a time step of 0.01h. We evaluated the model using the Root-Mean-Squared Error (RMSE) metric. The formula is given in Equation (11) where N denotes the number

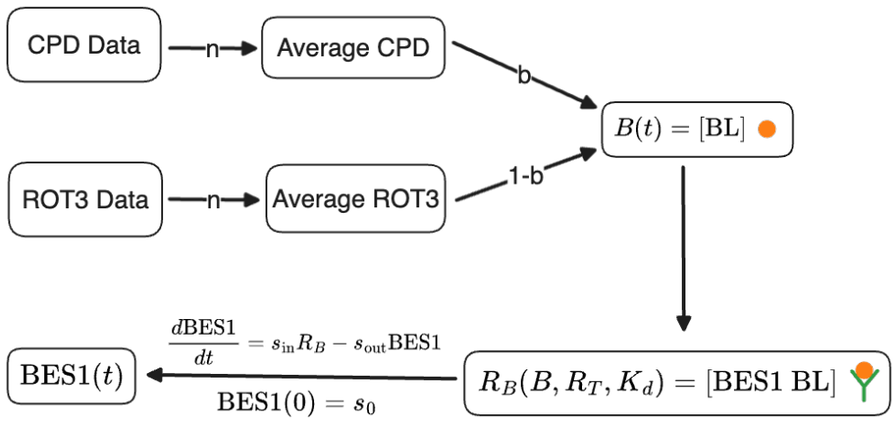

Figure 6: A visual depiction of the model up to this point. The extracellular BL concentration function $B(t)$ is computed using a moving biased average of the CPD and ROT3 biosynthetic enzymes. Then, $B(t)$ is used to determine the concentration of bound receptors R_B, building on the work of van Esse et al., 2012. Finally, an ordinary differential equation model is used to express the BES1 transcription factor as a function of time through R_B.

of observations. Each y_i $(1 \leq i \leq N)$ represents an observed value while each $f(t_i)$ denotes the model output at time t_i.

$$\mathrm{RMSE} = \sqrt{\frac{1}{N}\sum_{i=1}^{N}(y_i - f(t_i))^2} \tag{11}$$

Additionally, the Akaike Information Criterion (henceforth AIC) presented in Akaike, 1974 was used to compare the model presented (henceforth referred to as the complete model) with a linear and exponential regression on the BES1 signalling data. The AIC compares the relative quality of statistical models by considering both the goodness of fit and the informational complexity of the model.

$$\Delta\mathrm{AIC} = 2k + N \ln\left(\frac{1}{N}\sum_{i=1}^{N}(y_i - f(t_i))^2\right) \tag{12}$$

In the equation above, k denote the number of parameters in the model and N is the number of observations. Since the AIC is used to compare models its absolute value is irrelevant. Therefore, the ΔAIC values presented in the forthcoming plots may be rescaled by a fixed constant to improve readability. The `scipy.optimize.minimize` function from the scientific computation package scipy was used to determine the values of $s_0 \in [0, 0.5]$, $s_{\mathrm{in}} \in [0, 0.5]$, and $s_{\mathrm{out}} \in [0, 0.5]$ that yielded the lowest error. Searching a larger parameter space did not produce a better fit (not shown). Figure 7 compares the fitted model to the experimental data and Table 4.3 presents the optimized parameters.

Parameter	Value	Units
s_0	2.35×10^{-3}	BES1
s_{in}	4.79×10^{-2}	BES1/R_Bh
s_{out}	3.53×10^{-6}	1/h

The fitted parameter value $s_{\mathrm{out}} = 3.53 \times 10^{-6}$ appears to be unreasonably low in the biological context of the problem. It suggests that BES1 has a half life of around 150 days, which is unusually large. Narsai et al., 2007 found that the the half life of transcription factors in *A. thaliana* had a mean of 5.9h and a median of 3.8h. However, some transcription factors had half lives above 24h. With these findings in mind, we can expect that the true value of s_{out} is probably no more than 0.5 and no less than 0.01.

To check if our model still performed reasonably well for values of s_{out} within a biologically realistic range, we fixed s_0 to its fitted value and ran the model for a wide variety of possible s_{in} and s_{out} values. More precisely, we computed 100 evenly spaced points from $s_{\mathrm{in}} \in [0, 0.5]$ and 100 evenly spaced points from $s_{\mathrm{out}} \in [0, 0.5]$. This produced a lattice of 10 000 points in two-dimensional parameter space which

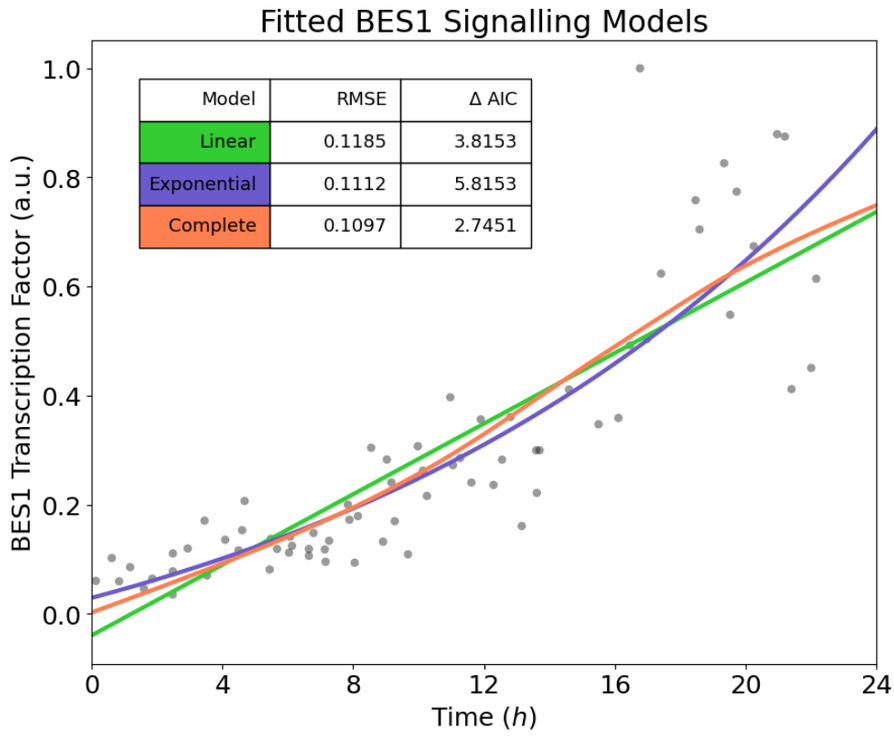

Figure 7: Results of model fitting to the BES1 signalling data from Vukašinović et al., 2021. The complete model was the best performing in terms of both absolute error and information-theoretic quality.

were used to evaluate the model. Then, we ran the model at each of these points and plotted in the errors in Figure 8.

While the fitted parameter value $s_{\text{out}} = 3.53 \times 10^{-6}$ is probably not the true half life of the BES1 transcription factor as discussed previously, the parameter space search shows that the model also performs reasonably well for values of s_{out} between 0.01 and 0.5. Lower values of s_{out}, which correspond with a longer BES1 half-life, produce slightly less error than higher values. This is indicated by the brighter yellow colour near the bottom of the dotted black line in Figure 8. In the regime where s_{out} is small Equation (10) can be approximated as follows:

$$\frac{\text{BES1}}{dt} = s_{\text{in}} R_B - s_{\text{out}}\text{BES1} \approx s_{\text{in}} R_B \Rightarrow \text{BES1} \approx s_{\text{in}} \int R_B \, dt \tag{13}$$

This approximation indicates that the BES1 transcription factor accumulates over time in the cell and does not reach the maximum steady state value imposed by s_{out}. All of the biologically reasonable values for s_{out} fall under this regime. For the sake of comparison, let us also consider the region of our parameter space where s_{out} is large, which produces a less accurate fit. Under this regime we have the following approximation for the BES1 function:

$$\text{BES1} = \frac{s_{\text{in}} R_B}{s_{\text{out}}} + \left(s_0 - \frac{s_{\text{in}} R_B}{s_{\text{out}}} \right) e^{-s_{\text{out}}\text{BES1}} \approx \frac{s_{\text{in}} R_B}{s_{\text{out}}}$$

When s_{out} is large, the BES1 transcription factor rapidly reaches its steady state value, and is thus approximately proportional to R_B over the domain. As mentioned previously, the actual system probably does not behaves this way since the model fits poorly to the data for larger values of s_{out}.

The results of the parameter space search shown in Figure 8 also indicate that if s_{in} or s_{out} can be determined through experiments, the other parameter value can also be estimated to a high degree of accuracy using the linear relationship $s_{\text{out}} = L(s_{\text{in}}) = 2.200 s_{\text{in}} - 0.089$. This result is significant because it may be experimentally feasible to find s_{out}, the BES1 transcription factor decay constant, and use it to determine s_{in}, which would be difficult to determine experimentally. However, there are some caveats to this approach. Since the data has arbitrary units, quantifying s_{in} would also require making exact measurements of the BES1 transcription factor and using them to rescale Equation (10) prior to using the linear relationship we identified. Additionally, there is some uncertainty in the behaviour

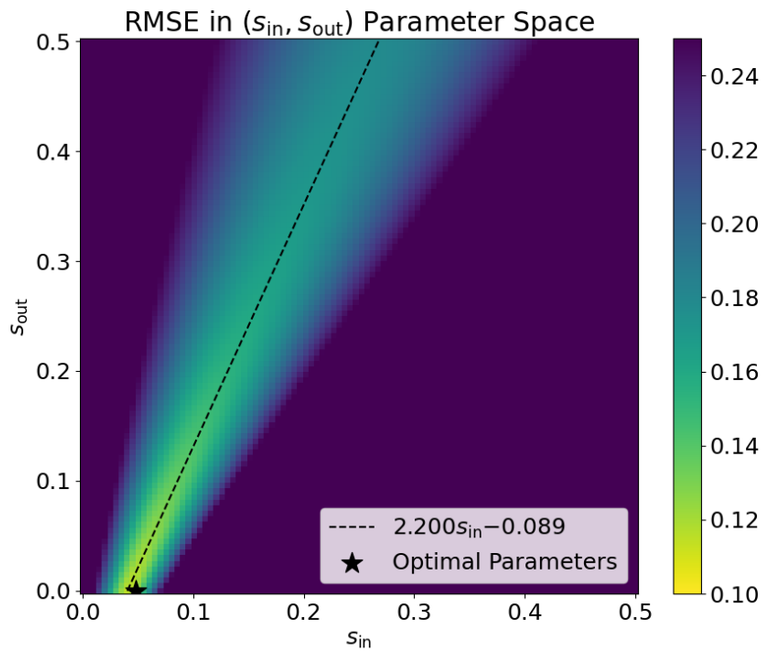

Figure 8: Heatmap showing the model RMSE for a 100×100 grid of $(s_{\text{in}}, s_{\text{out}})$ parameter values. The initial condition s_0 was fixed to its fitted value of 2.35×10^{-3}. Regions of the plot shaded dark purple were truncated to an RMSE of 0.25 and thus the actual RMSE at these points may be higher. The results of this process indicate a clear linear relationship between s_{in} and s_{out} which is given approximately by the linear function function $s_{\text{out}} = L(s_{\text{in}}) = 2.200 s_{\text{in}} - 0.089$.

of the BL concentration function $B(t)$ as the exact details of the BL biosynthetic pathway were left out of the model. That being said, the scale scale of the BL concentration ($\approx 1\text{nmol}\,\text{L}^{-1}$) is grounded in the literature (van Esse et al., 2012).

5 Single Cell Mutant Model

6 Discussion

6.1 The Single Cell Model

Many of the parameters presented were prescribed or assigned prior to fitting the model. Some of these parameters, such as K_d (the BL dissociation constant) and R_T (the total concentration of BRI1 receptors) were based on previous results in the literature. However, other parameters such as n (the BL moving average period) and b (the CPD/ROT3 bias) were prescribed with minimal justification. This was necessary due to the fact that the data available was only able to support a small number of parameters without running the risk of overfitting. In light of new data, it may be possible to get estimates and confidence intervals for the assigned parameters.

Further experiments are necessary to more accurately fit the model. In particular, quantitative measurements of extracellular BR concentrations, CLASP protein levels, and the BES1 transcription factor would lead to significant improvements in model efficacy. The work in this paper also presents interesting oppourtunities for further modelling. Adding a model of cell division to the system of ODEs presented here would make it possible to describe an entire column of trichoblast or atrichoblast cells. This cell column model could be integrated into a two-dimensional cross section model (Grieneisen et al., 2007, Di Mambro et al., 2017, Salvi et al., 2020), which often omit the effects of BR and CLASP on growth and division. This would make it possible to study the crosstalk between BR and auxin (Chaiwanon and Wang, 2015, Vragović et al., 2015) *in silico* to help us better understand how these crucial plant hormones interact with one another.

6.2 Data Limitations

We developed models of cell growth using time-dependent ODEs but soon realized that such models could not be extended to the CLASP-1 and BRIN-CLASP mutants. The reason for this is that the data from Goh et al., 2023 was crucial for converting position-dependent observations into time-dependent observations. However, this data was taken from wild type roots, and the position vs. time function we approximated is likely different for the mutants. In order to validate the time-dependent models presented in the previous section with experimental data, we would need multiple images of the CLASP-1 and BRIN-CLASP root tips over a period of time. Unfourtunately, this data is not currently available.

A Supplementary Information

A.1 Quantifying Differences Between Mutants

The raw data on the mutant roots presented in Figure 2 is in units of cell number versus cell length. The data was gathered from approximately 30 cell columns per mutant, with each column originating from a different plant. We transformed this data into units of time and length using the following procedure. First, we made the assumption that cells are perfect cylinders, so that their cross sectional area is equal to their length multiplied by their diameter. Then, we assumed that the diameter of each cell is identical, and prescribed a suitably chosen diameter $d = 10\mu$m based on experimental data (Goh et al., 2023). To convert cell number to position we took the cumulative sum of the cell lengths over each cell column. Missing data was filled in using the average length for that cell number and mutant. The results of this data preprocessing is shown in Figure 1.

We wish to quantify the differences between the mutants in order to confirm that their behaviour is indeed different from the wild type. To do this, we computed the relative error of each data point from the line of best fit for the wild type cells. The distribution of these errors is shown in Figure 2. Cells in the BRIN-CLASP root have a mean error of +41% from the wild type average, while cells in the CLASP-1 root have a mean error of +80.9%. This suggests a significant effect size for the various mutations. Additionally, the mutations were statistically significant with p-values less than 10^{-20}, which provides further evidence that the mutants are exhibiting different behaviour.

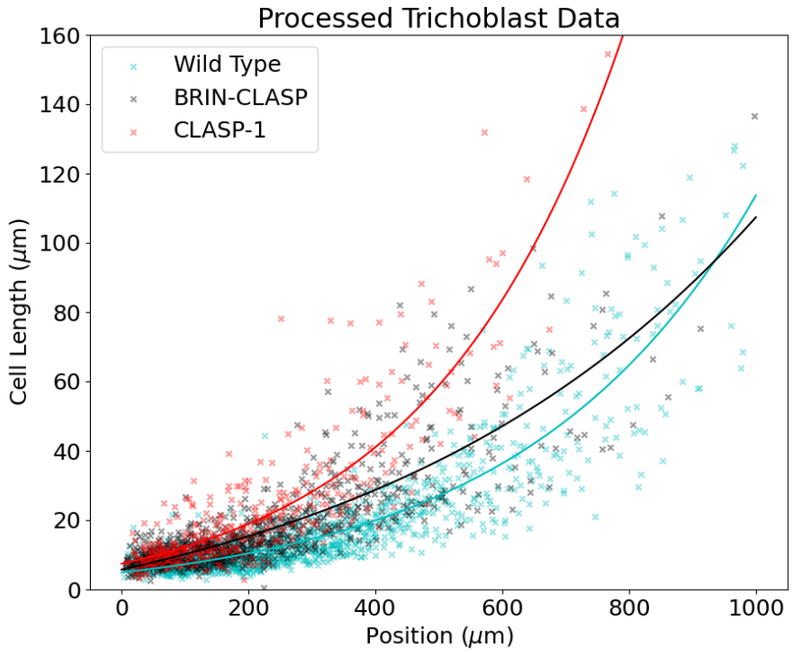

Supplementary Figure 1: Plot of cell lengths from trichoblast cells in wild type, CLASP-1, and BRIN-CLASP roots. The line of best fit is an exponential function of the form $A + Be^{Cx}$. Wild type cells are on average the shortest, followed closely by BRIN-CLASP. CLASP-1 cells are significantly longer, especially in the proximal regions of the root. There is a large amount of variance in the data, especially at higher positions.

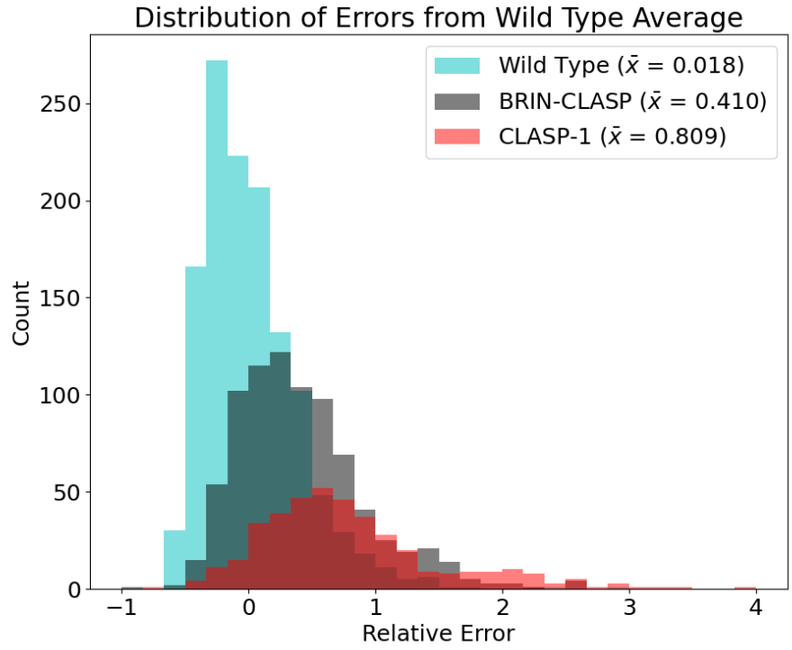

Supplementary Figure 2: Distribution of errors from the wild type average presented in Figure 1. The mean error of the BRIN-CLASP and CLASP-1 mutants are clearly positive, which suggests that on average, the mutants have longer cells compared to the wild type.

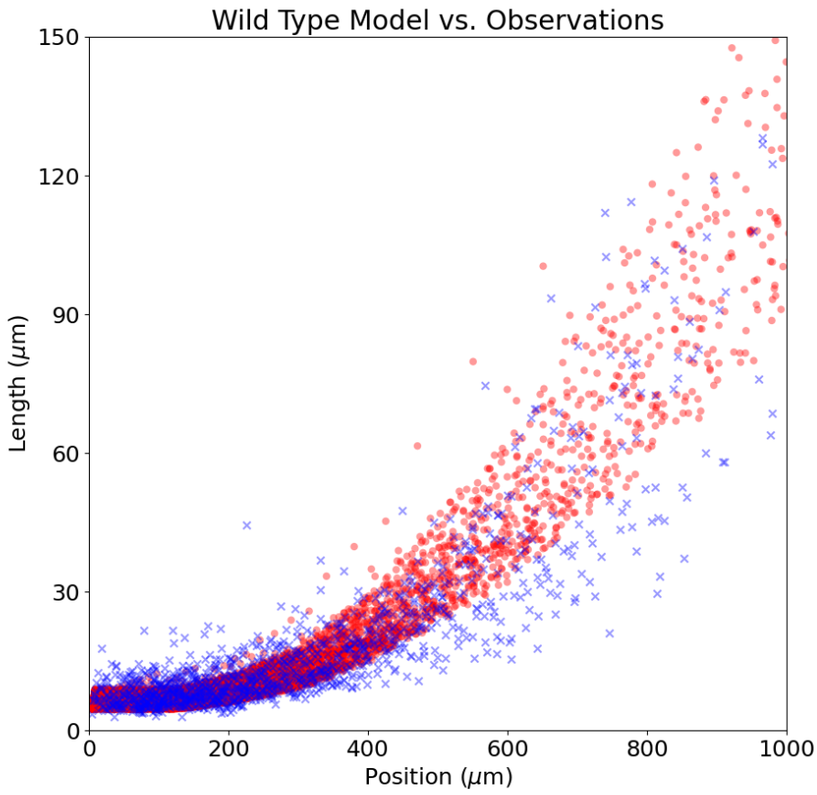

Supplementary Figure 3: Comparison of wild type cell column model with observations.

A.2 Cell Column Model

A.3 Single Cell BES1 Model

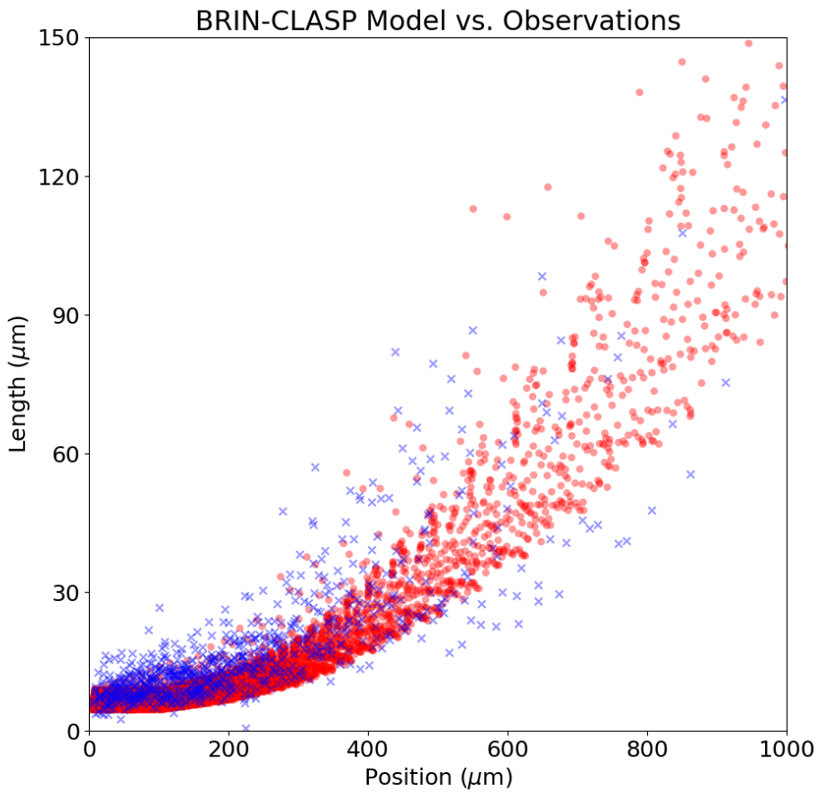

Supplementary Figure 4: Comparison of BRIN-CLASP cell column model with observations.

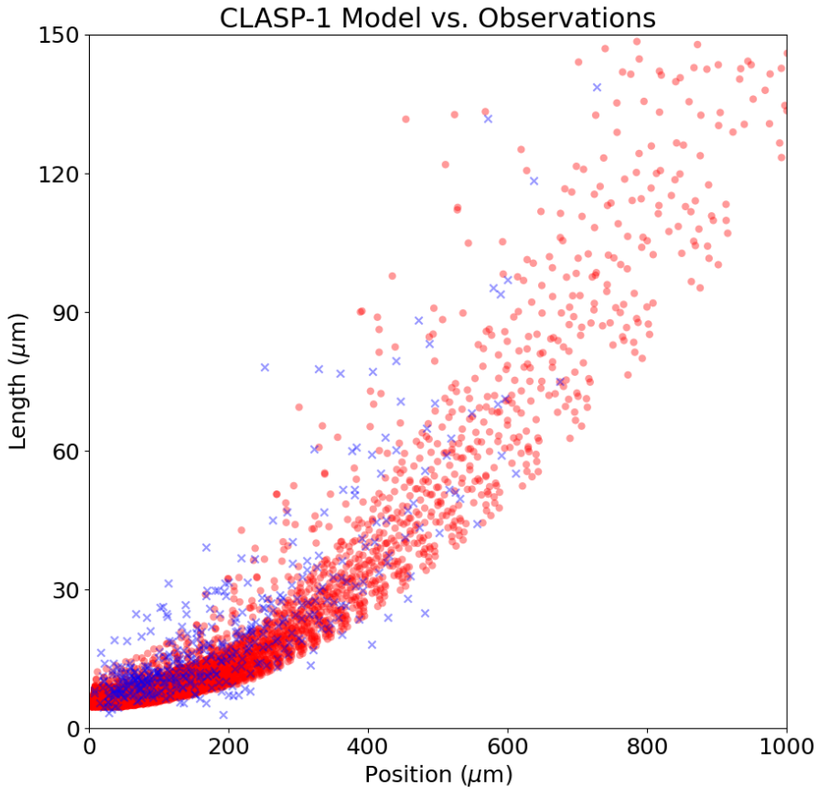

Supplementary Figure 5: Comparison of CLASP-1 cell column model with observations.

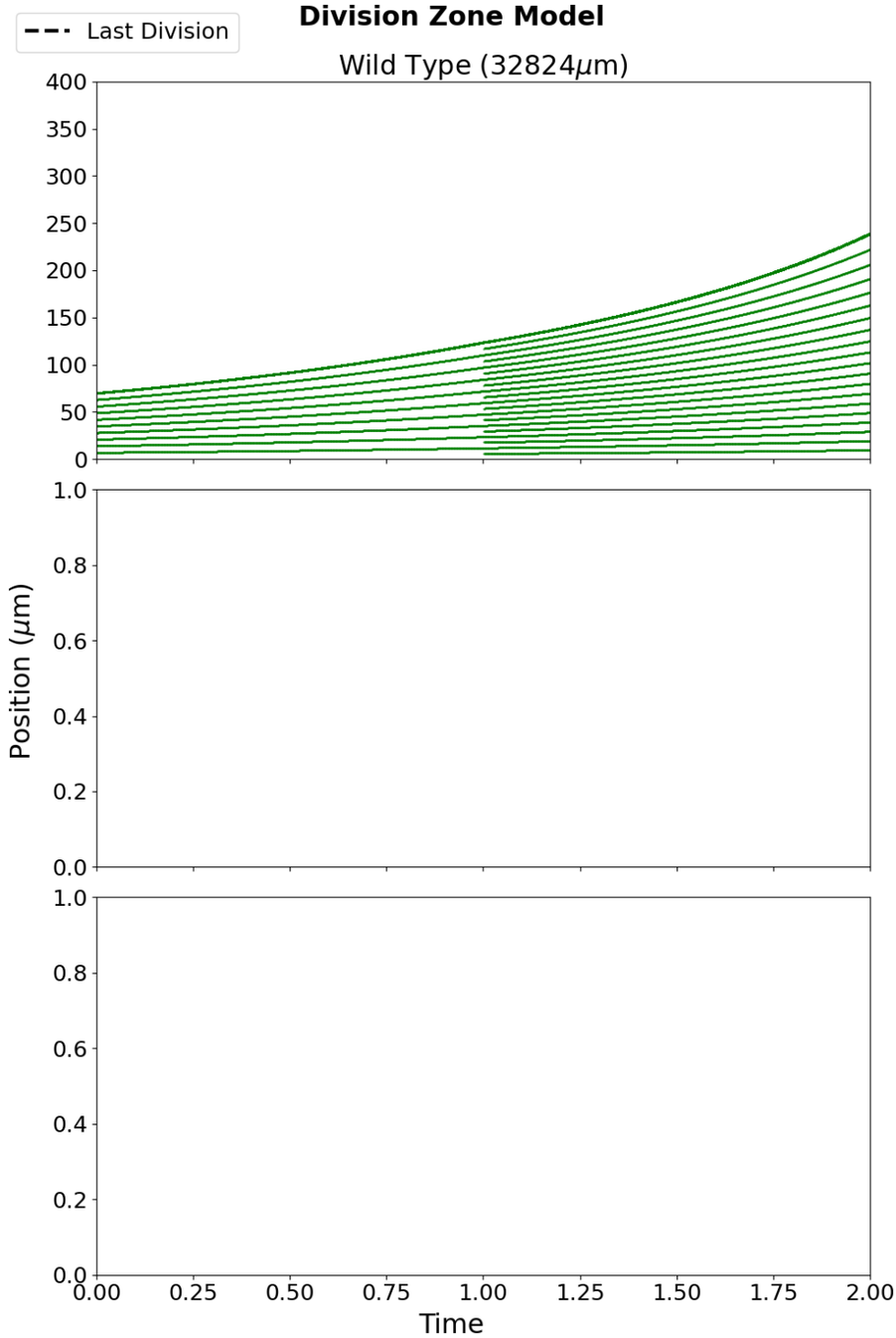

Supplementary Figure 6: A plot of the simulated cells in the division zone.

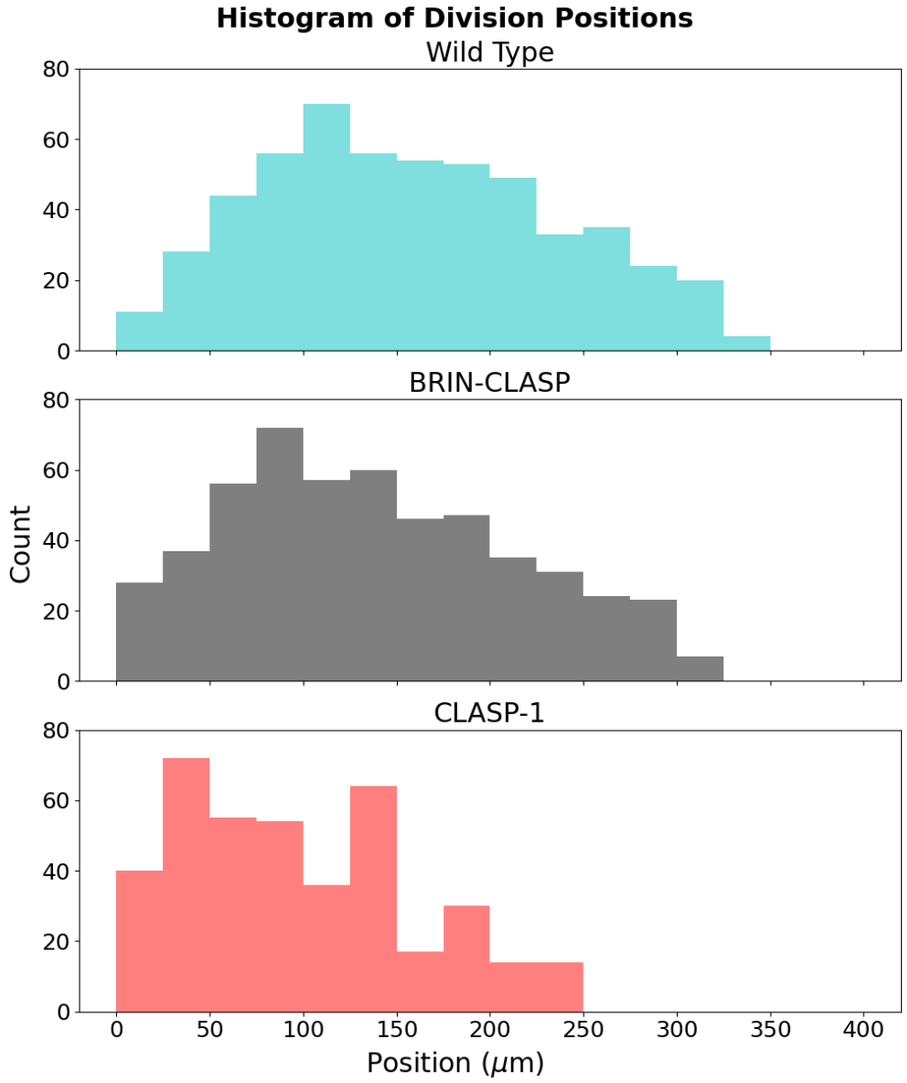

Supplementary Figure 7: A histogram of division positions in each the two mutants and wild type.

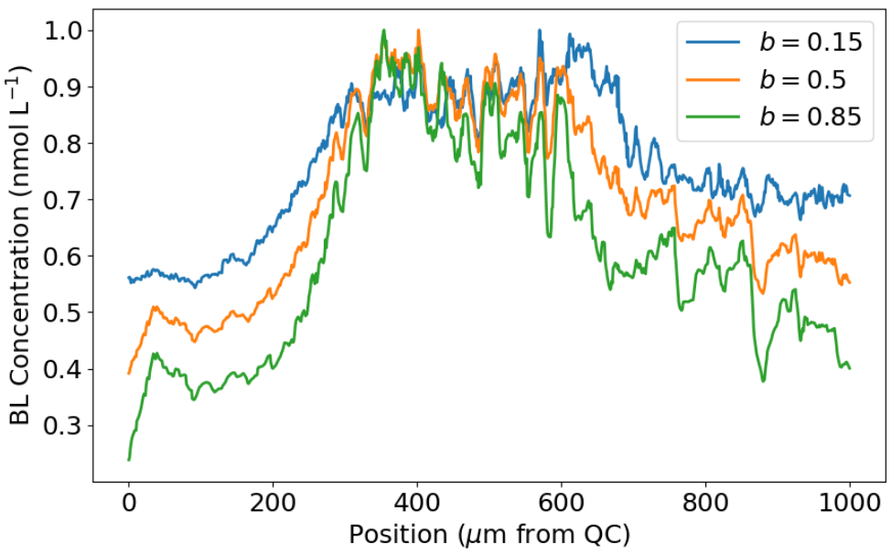

Supplementary Figure 8: The BL concentration function for three different values of the bias parameter b. For future simulations we will use $b = 0.5$, since the BL concentration function exhibits similar qualitative behaviour for all b as shown above.

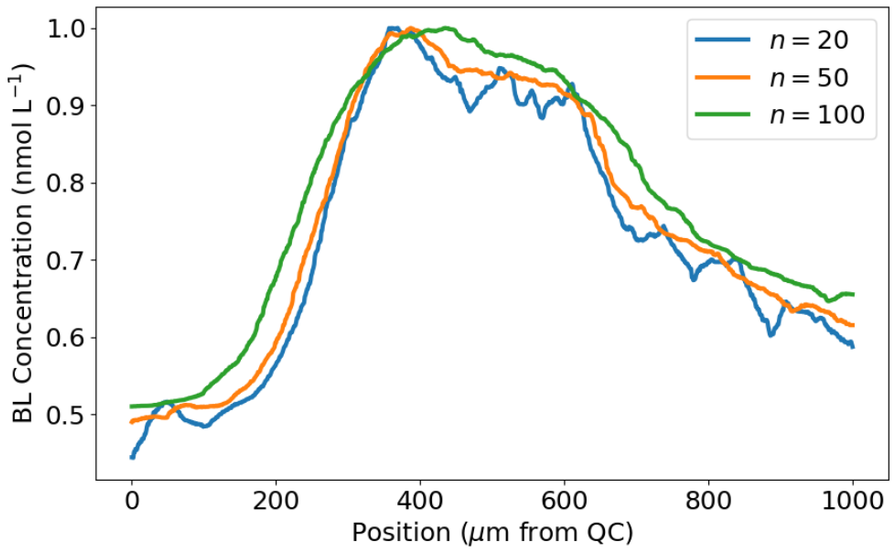

Supplementary Figure 9: A plot of BL concentration functions ($b = 0.5$) for three different values of the moving average period n. Future simulations will use $n = 50$, an admittedly arbitrary choice since the exact details of the diffusive effect we are modelling are unknown.

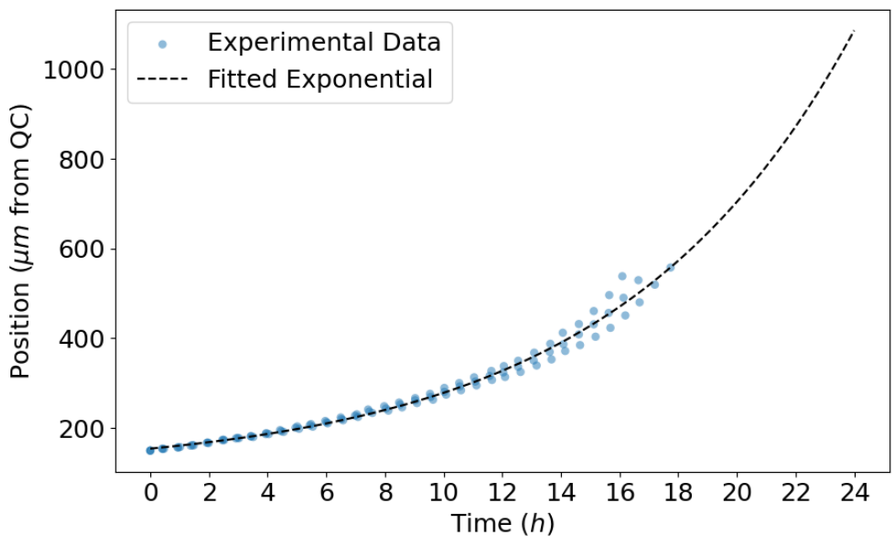

Supplementary Figure 10: Plot of cell position (in µm) versus time (in h) using cell lineage data from Goh et al., 2023. The function is scaled such that $t = 0$h corresponds to a position of 150µm above the QC.

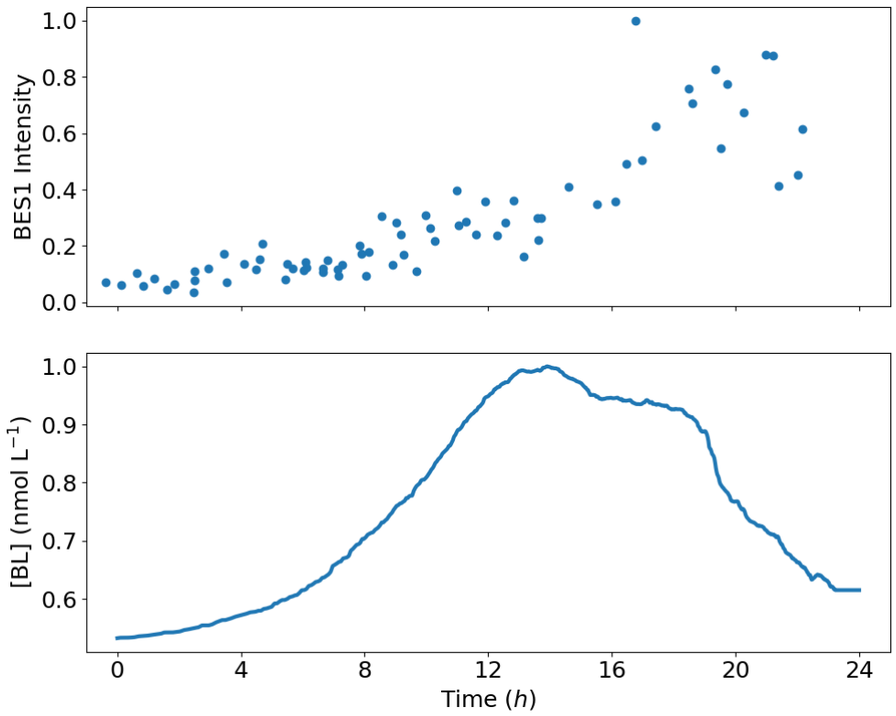

Supplementary Figure 11: Plot of the transformed BES1 signalling data from Vukašinović et al., 2021 (left) and transformed BL concentration function (right). Since fluorescence intensity data is measured in arbitrary units, the BES1 plot was rescaled to a maximum value of 1.

References

Akaike, H. (1974). A new look at the statistical model identification. *IEEE Transactions on Automatic Control*, *19*(6), 716–723. https://doi.org/10.1109/TAC.1974.1100705

Wang, Z.-Y., Seto, H., Fujioka, S., Yoshida, S., & Chory, J. (2001). BRI1 is a critical component of a plasma-membrane receptor for plant steroids. *Nature*, *410*(6826), 380–383. https://doi.org/10.1038/35066597

Caño-Delgado, A., Yin, Y., Yu, C., Vafeados, D., Mora-García, S., Cheng, J.-C., Nam, K. H., Li, J., & Chory, J. (2004). BRL1 and BRL3 are novel brassinosteroid receptors that function in vascular differentiation in Arabidopsis. *Development (Cambridge, England)*, *131*(21), 5341–5351. https://doi.org/10.1242/dev.01403

Verbelen, J.-P., Cnodder, T. D., Le, J., Vissenberg, K., & Baluška, F. (2006). The Root Apex of *Arabidopsis thaliana* Consists of Four Distinct Zones of Growth Activities: Meristematic Zone, Transition Zone, Fast Elongation Zone and Growth Terminating Zone. *Plant Signaling & Behavior*, *1*(6), 296–304. https://doi.org/10.4161/psb.1.6.3511

Ambrose, J. C., Shoji, T., Kotzer, A. M., Pighin, J. A., & Wasteneys, G. O. (2007). The Arabidopsis CLASP Gene Encodes a Microtubule-Associated Protein Involved in Cell Expansion and Division. *The Plant Cell*, *19*(9), 2763–2775. https://doi.org/10.1105/tpc.107.053777

Grieneisen, V. A., Xu, J., Marée, A. F. M., Hogeweg, P., & Scheres, B. (2007). Auxin transport is sufficient to generate a maximum and gradient guiding root growth. *Nature*, *449*(7165), 1008–1013. https://doi.org/10.1038/nature06215

Narsai, R., Howell, K. A., Millar, A. H., O'Toole, N., Small, I., & Whelan, J. (2007). Genome-Wide Analysis of mRNA Decay Rates and Their Determinants in Arabidopsis thaliana. *The Plant Cell*, *19*(11), 3418–3436. https://doi.org/10.1105/tpc.107.055046

Hamant, O., & Traas, J. (2010). The mechanics behind plant development. *New Phytologist*, *185*(2), 369–385. https://doi.org/10.1111/j.1469-8137.2009.03100.x

Ambrose, C., Allard, J. F., Cytrynbaum, E. N., & Wasteneys, G. O. (2011). A CLASP-modulated cell edge barrier mechanism drives cell-wide cortical mi-

crotubule organization in Arabidopsis. *Nature Communications*, *2*(1), 430. https://doi.org/10.1038/ncomms1444

van Esse, G. W., van Mourik, S., Stigter, H., ten Hove, C. A., Molenaar, J., & de Vries, S. C. (2012). A Mathematical Model for BRASSINOSTEROID INSENSITIVE1-Mediated Signaling in Root Growth and Hypocotyl Elongation. *Plant Physiology*, *160*(1), 523–532. https://doi.org/10.1104/pp.112.200105

Chaiwanon, J., & Wang, Z.-Y. (2015). Spatiotemporal Brassinosteroid Signaling and Antagonism with Auxin Pattern Stem Cell Dynamics in Arabidopsis Roots. *Current Biology*, *25*(8), 1031–1042. https://doi.org/10.1016/j.cub.2015.02.046

Kumpf, R. P., & Nowack, M. K. (2015). The root cap: A short story of life and death. *Journal of Experimental Botany*, *66*(19), 5651–5662. https://doi.org/10.1093/jxb/erv295

Vragović, K., Sela, A., Friedlander-Shani, L., Fridman, Y., Hacham, Y., Holland, N., Bartom, E., Mockler, T. C., & Savaldi-Goldstein, S. (2015). Translatome analyses capture of opposing tissue-specific brassinosteroid signals orchestrating root meristem differentiation. *Proceedings of the National Academy of Sciences*, *112*(3), 923–928. https://doi.org/10.1073/pnas.1417947112

Di Mambro, R., De Ruvo, M., Pacifici, E., Salvi, E., Sozzani, R., Benfey, P. N., Busch, W., Novak, O., Ljung, K., Di Paola, L., Marée, A. F. M., Costantino, P., Grieneisen, V. A., & Sabatini, S. (2017). Auxin minimum triggers the developmental switch from cell division to cell differentiation in the Arabidopsis root. *Proceedings of the National Academy of Sciences*, *114*(36), E7641–E7649. https://doi.org/10.1073/pnas.1705833114

Pavelescu, I., Vilarrasa-Blasi, J., Planas-Riverola, A., González-García, M.-P., Caño-Delgado, A. I., & Ibañes, M. (2018). A Sizer model for cell differentiation in Arabidopsis thaliana root growth. *Molecular Systems Biology*, *14*(1), e7687. https://doi.org/10.15252/msb.20177687

Ruan, Y., Halat, L. S., Khan, D., Jancowski, S., Ambrose, C., Belmonte, M. F., & Wasteneys, G. O. (2018). The Microtubule-Associated Protein CLASP Sustains Cell Proliferation through a Brassinosteroid Signaling Negative Feedback Loop. *Current Biology*, *28*(17), 2718–2729.e5. https://doi.org/10.1016/j.cub.2018.06.048

Ackerman-Lavert, M., & Savaldi-Goldstein, S. (2020). Growth models from a brassinosteroid perspective. *Current Opinion in Plant Biology*, *53*, 90–97. https://doi.org/10.1016/j.pbi.2019.10.008

Salvi, E., Rutten, J. P., Mambro, R. D., Polverari, L., Licursi, V., Negri, R., Ioio, R. D., Sabatini, S., & Tusscher, K. T. (2020). A Self-Organized PLT/Auxin/ARR-B Network Controls the Dynamics of Root Zonation Development in Arabidopsis thaliana. *Developmental Cell*, *53*(4), 431–443.e23. https://doi.org/10.1016/j.devcel.2020.04.004

Matosevich, R., & Efroni, I. (2021). The quiescent center and root regeneration. *Journal of Experimental Botany*, *72*(19), 6739–6745. https://doi.org/10.1093/jxb/erab319

Vukašinović, N., Wang, Y., Vanhoutte, I., Fendrych, M., Guo, B., Kvasnica, M., Jiroutová, P., Oklestkova, J., Strnad, M., & Russinova, E. (2021). Local brassinosteroid biosynthesis enables optimal root growth. *Nature Plants*, *7*(5), 619–632. https://doi.org/10.1038/s41477-021-00917-x

Halat, L. S., Bali, B., & Wasteneys, G. (2022). Cytoplasmic Linker Protein-Associating Protein at the Nexus of Hormone Signaling, Microtubule Organization, and the Transition From Division to Differentiation in Primary Roots. *Frontiers in Plant Science*, *13*. https://doi.org/10.3389/fpls.2022.883363

Goh, T., Song, Y., Yonekura, T., Obushi, N., Den, Z., Imizu, K., Tomizawa, Y., Kondo, Y., Miyashima, S., Iwamoto, Y., Inami, M., Chen, Y.-W., & Nakajima, K. (2023). In-Depth Quantification of Cell Division and Elongation Dynamics at the Tip of Growing Arabidopsis Roots Using 4D Microscopy, AI-Assisted Image Processing and Data Sonification. *Plant and Cell Physiology*, *64*(11), 1262–1278. https://doi.org/10.1093/pcp/pcad105